Supplementary Information

Single Iron Site Catalysts with Increased Metal-Site Loading via High-Temperature Imprinting Approach for Proton Exchange Membrane Fuel Cells

Xinhong Liang,[abc] Pengwei Zhao,[d] Zhiyuan Gao,[abc] Jiashun Liang,[e] Xiaoxuan Yang,[e] Kai Ao,[abc] Jianwen Zhu,[abc] Yi Mei,[abc] Gang Wu,*[e] and Yuanzhi Zhu*[abc]

[a] Faculty of Chemical Engineering, Kunming University of Science and Technology, Kunming 650500, P. R. China.

[b] Yunnan Provincial Key Laboratory of Energy Saving in Phosphorus Chemical Engineering and New Phosphorus Materials, Kunming 650500, P. R. China.

[c] Yunnan technological innovation center of phosphorus resources, Kunming 650600, P. R. China.

[d] School of Chemical Engineering and Technology, State Key Laboratory of Chemical Engineering, Collaborative Innovation Center of Chemical Science and Engineering, Tianjin University, Tianjin, 300072, China.

[e] Department of Chemical and Biological Engineering, University at Buffalo, The State University of New York, Buffalo, New York 14260, USA.

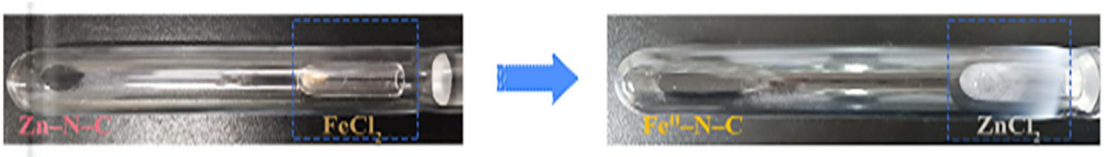

Figure S1. Schematic diagram of the experimental preparation of Fe^{II}–N–C catalyst.

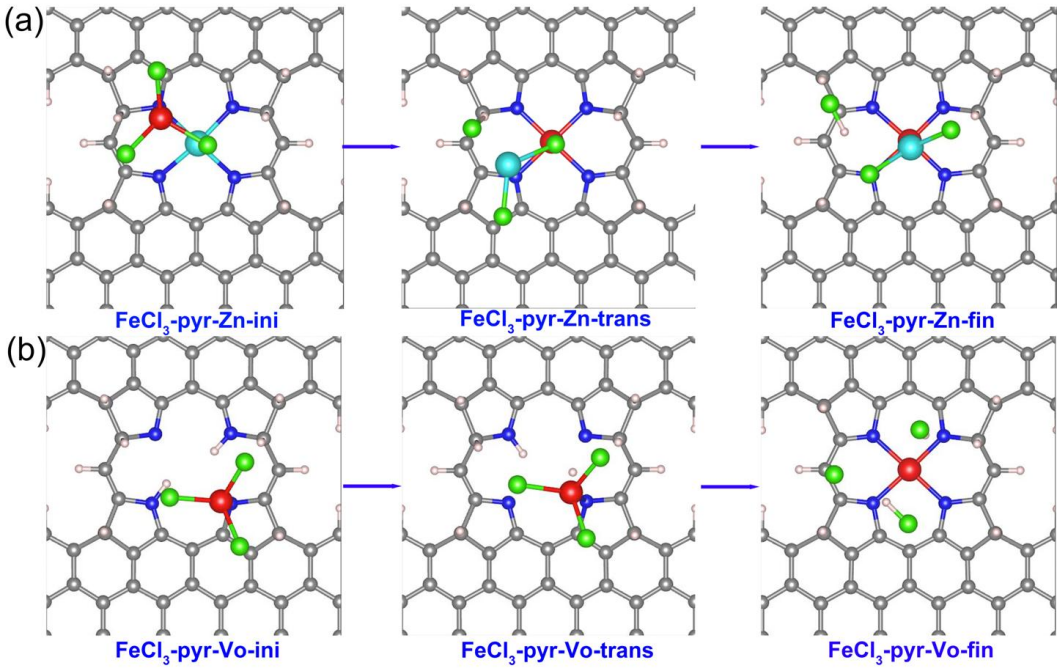

Figure S2. (a–b) The DFT theoretical calculation model for reactions between (a) $FeCl_3$ + ZnN_4 + H, and (b) $FeCl_3$ + V-N_4 + 3H.

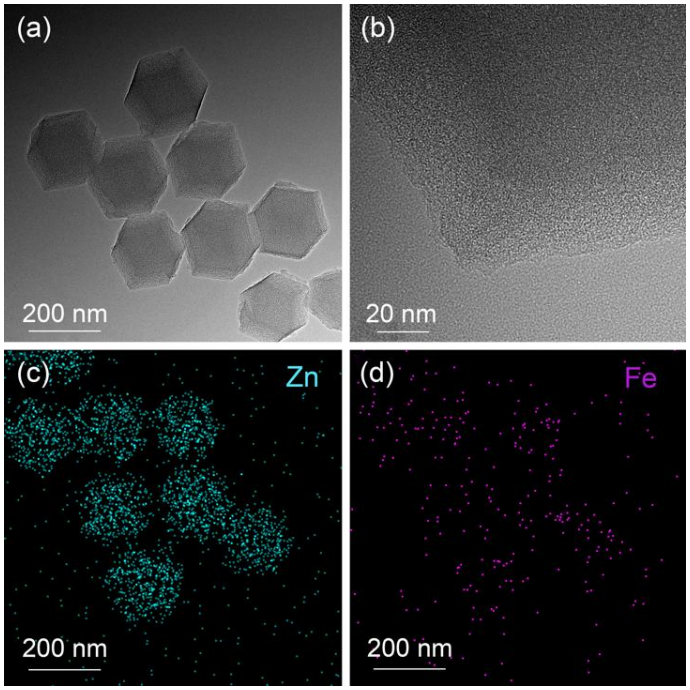

Figure S3. (a–b) TEM images of the Fe–N/C catalyst. representative TEM images of Zn–N–C catalyst at different magnifications. It can be clearly seen, while there are some slightly graphitic domains there are no particulate or encapsulated particulate phases visible. (c) Mapping images of Zn atoms. (d) Mapping images of Fe atoms.

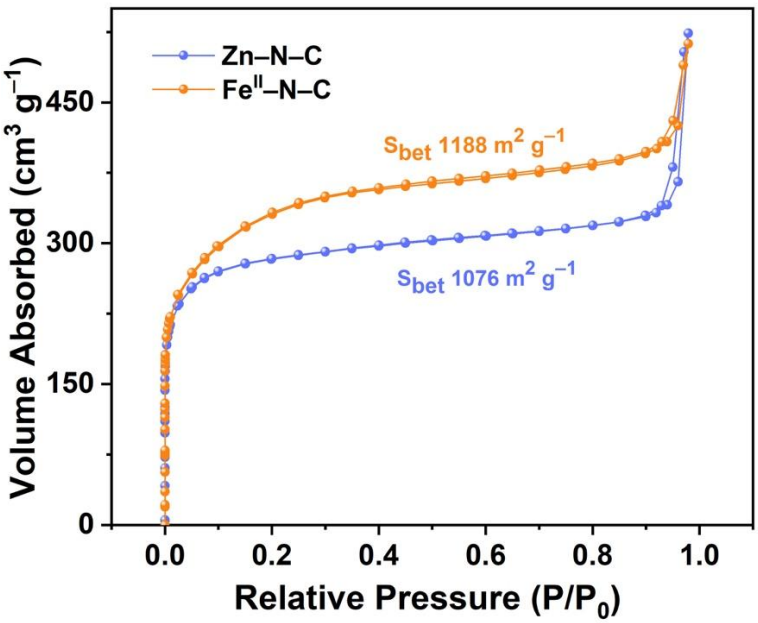

Figure S4. Pore volume size distribution of Zn–N–C and Fe^{II}–N–C catalyst.

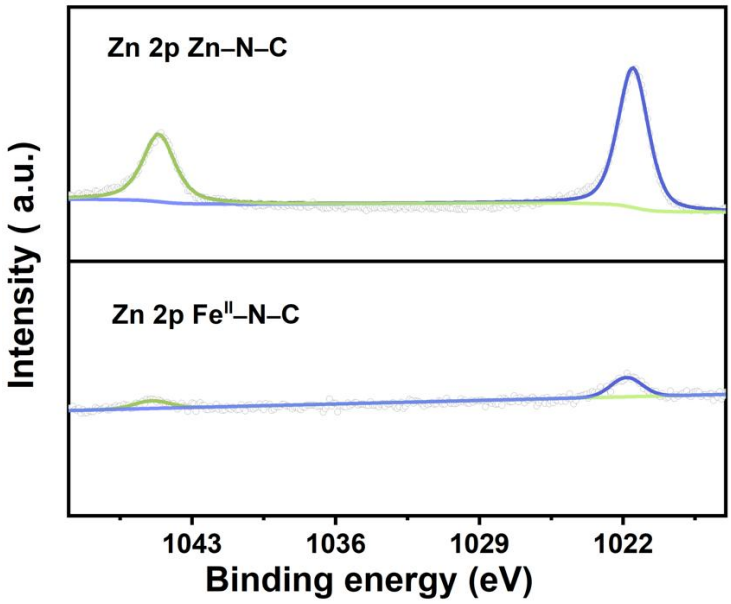

Figure S5. Zn 2p XPS spectra of Zn–N–C and FeII–N–C, revealing the presence of a Zn2+ 2p1/2 at 1021.6 eV and Zn2+ 2p3/2 at 1044.3 eV. It should be noticed that the Zn signal of FeII–N–C is significantly reduced.

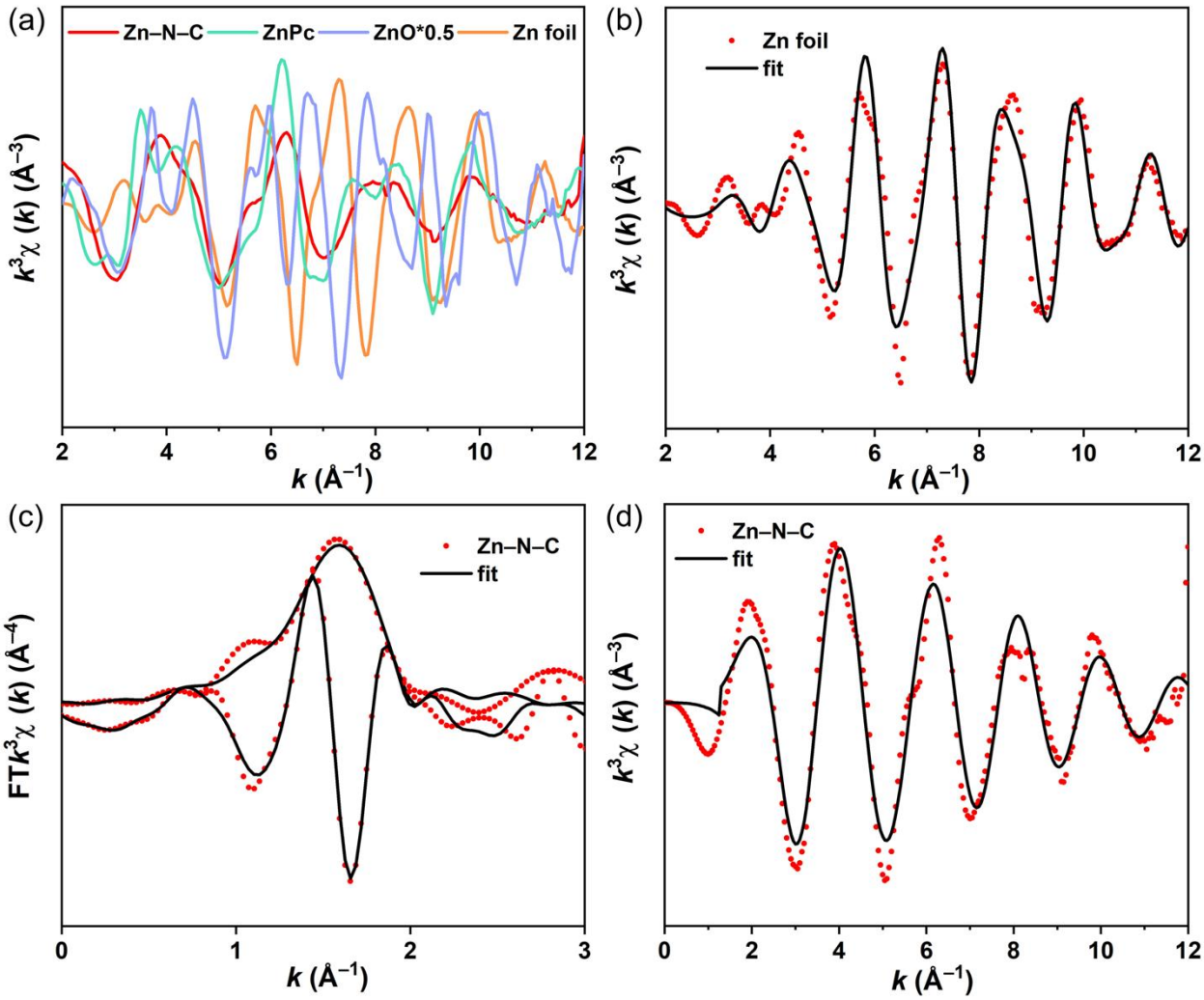

Figure S6. (a) K-space comparison of Zn–N–C, ZnPc, ZnO and Zn foil. (b) EXAFS analysis of Zn foil in K space. (c) EXAFS analysis of Zn–N–C in K space and R space. (d) EXAFS analysis of Zn–N–C in K space. The fitted EXAFS parameters are reported in Table S2.

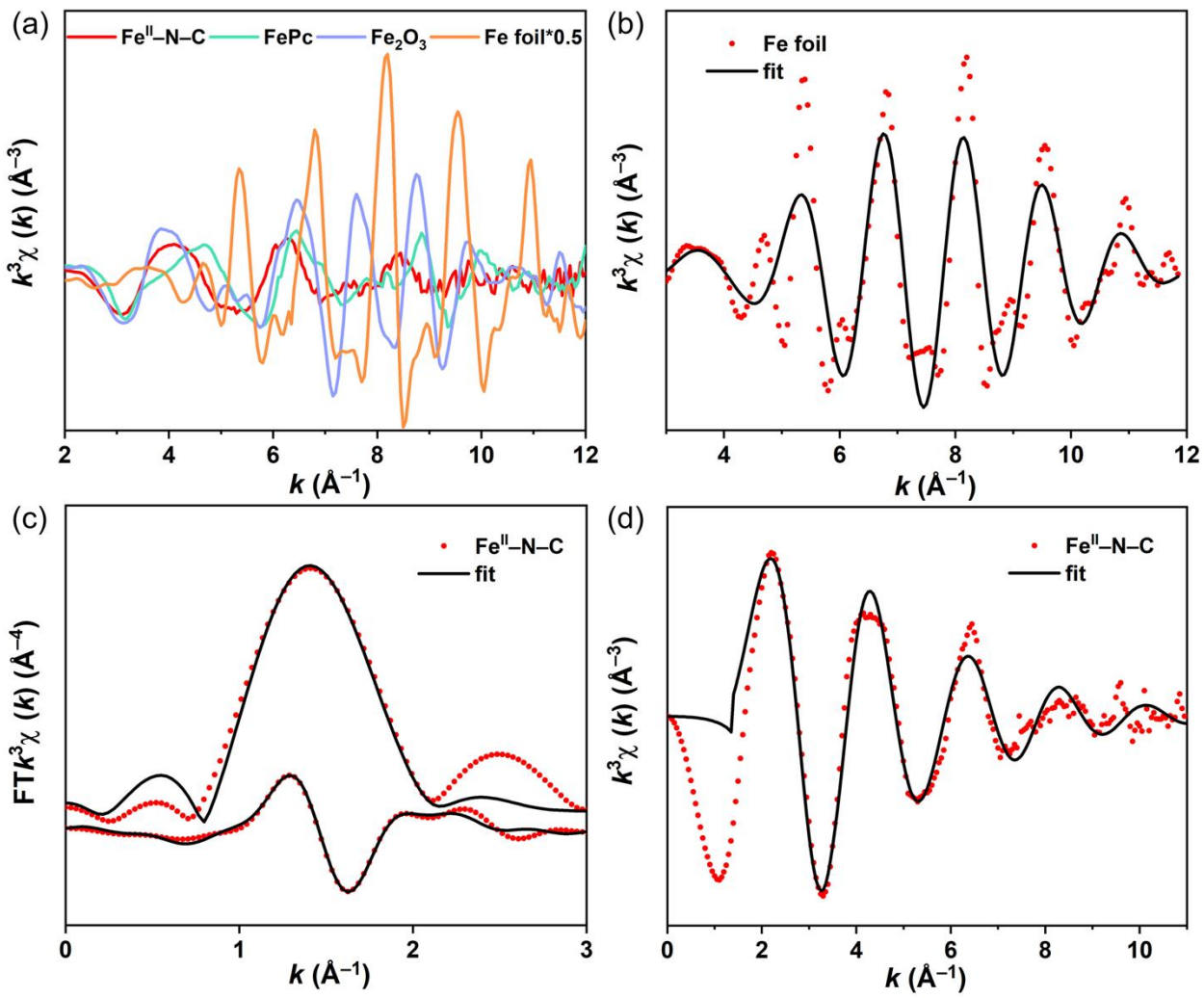

Figure S7. (a) K-space comparison of Fe^{II}–N–C, FePc, Fe_2O_3 and Fe foil. (b) EXAFS analysis of Fe foil in K space. (c) EXAFS analysis of FeII–N–C in K space and R space. (d) EXAFS analysis of FeII–N–C in K space. The fitted EXAFS parameters are reported in Table S2.

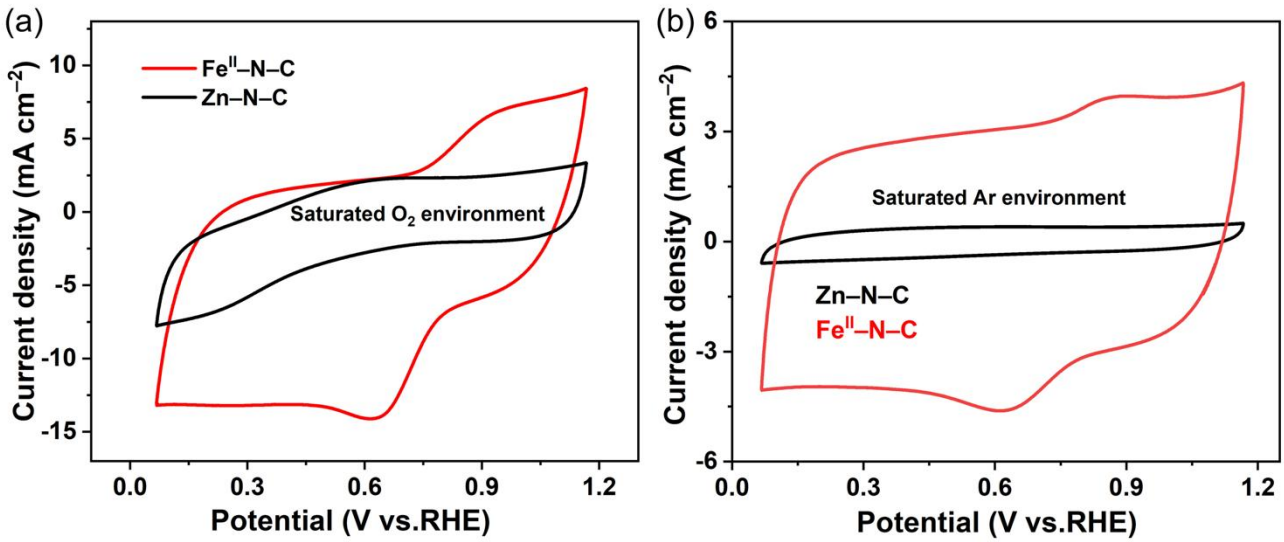

Figure S8. (a) Cyclic voltammetry curve of Zn–N–C and Fe^{II}–N–C catalysts in oxygen saturated solution at scan rate of 10 mV s^{-1}. (b) Cyclic voltammetry curves of Zn–N–C and Fe^{II}–N–C catalysts in argon-saturated solutions at scan rate of 10 mV s^{-1}.

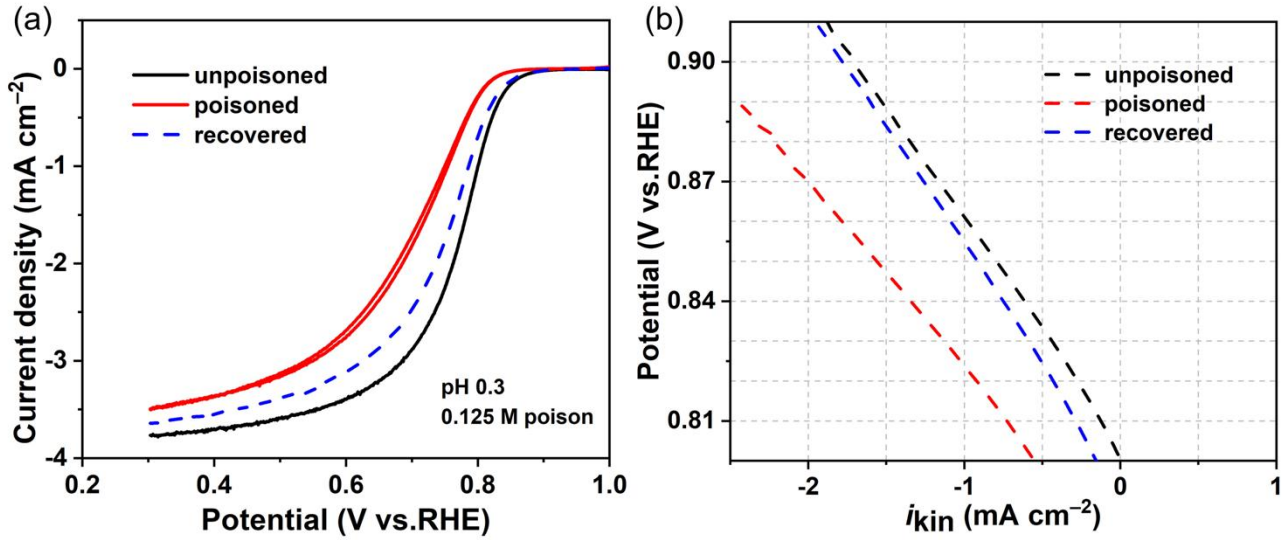

Figure S9. (a) Poisoning of the Fe^{II}–N–C catalyst in a 0.5 M H_2SO_4 electrolyte. Rotating disk electrode measurement of Fe^{II}–N–C catalyst before and after poisoning and recovery. Loading: 0.27 mg cm^{-2}, 1600 rpm, O_2-saturated electrolyte, 0.5 M H_2SO_4, 5 mV s^{-1}. Data in this figure show the effect of the poisoning protocol on the performance in 0.5M H_2SO_4. (b) Kinetic currents. Loading: 0.27 mg cm^{-2}, 1600 rpm, O_2-saturated electrolyte, 0.5M H_2SO_4, pH 0.3, 5 mV s^{-1}.

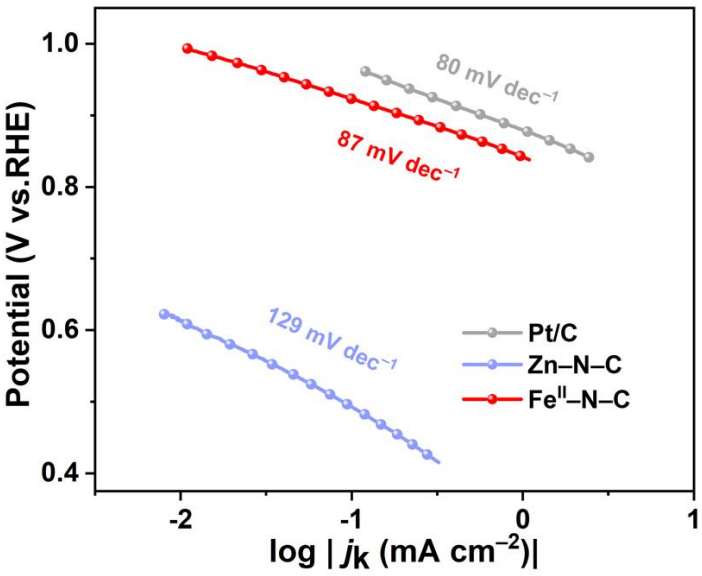

Figure S10. Tafel slope plots for Zn–N–C, commercial Pt/C and Fe^{II}–N–C.

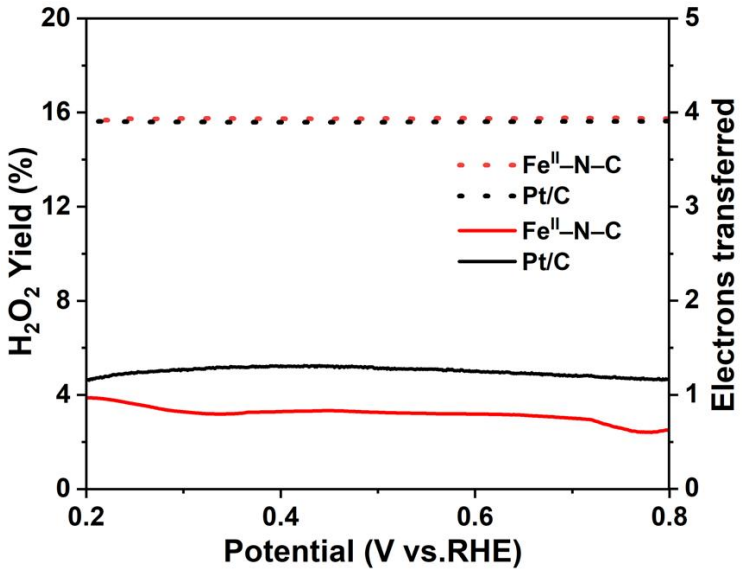

Figure S11. Number of transferred electrons and hydrogen peroxide yield of commercial Pt/C and Fe^{II}–N–C.

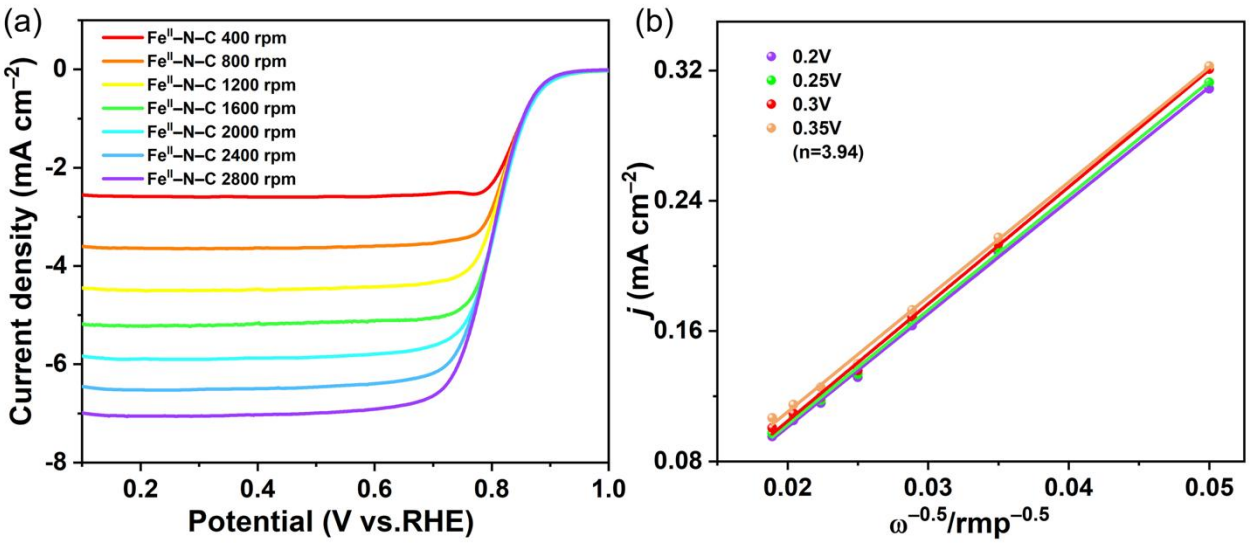

Figure S12. (a–b) Liner sweep voltammetry (LSV) curves and the corresponding Koutecky-Levich (K-L) plots of FeII–N–C at 400 to 2800 rpm rotation rates, a scan rate of 5 mV s^{-1}.

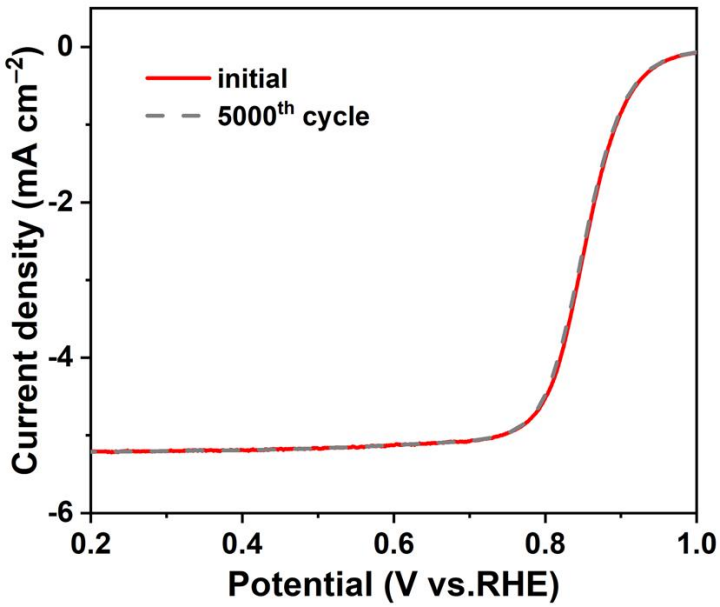

Figure S13. ORR polarization curves of Fe^{II}–N–C (using $FeCl_2$ as precursor) in an O_2-saturated 0.1M $HClO_4$ electrolyte. All tests were carried out on RDE with 1600 rpm rotating rate.

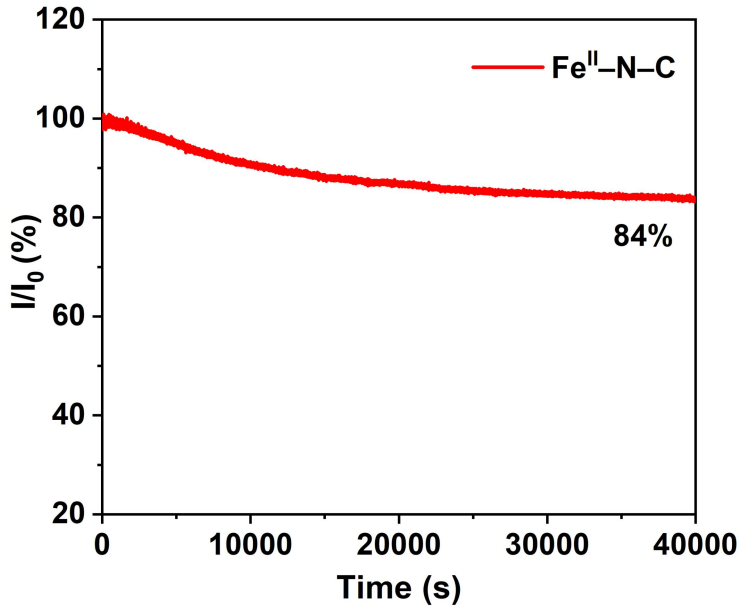

Figure S14. Chronoamperometry tests of Fe^{II}–N–C (using $FeCl_2$ as precursor) in an O_2-saturated 0.1M $HClO_4$ electrolyte.

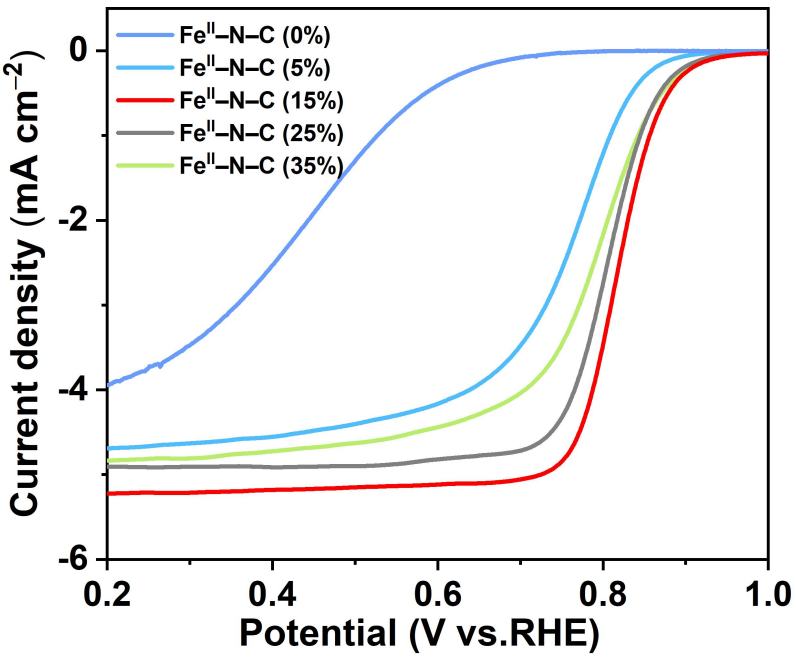

Figure S15. Exploration of the optimal metal addition to the Fe^{II}–N–C precursor.

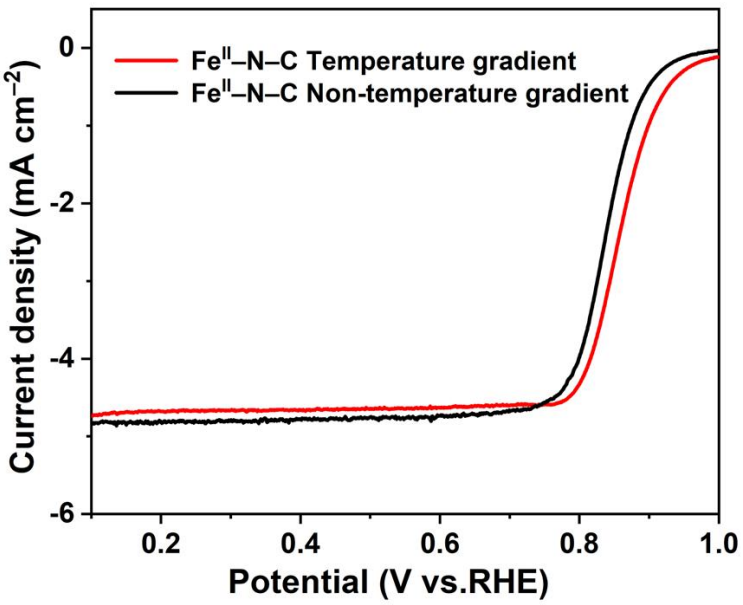

Figure S16. ORR polarization curves of Fe^{II}–N–C (using $FeCl_2$ as precursor) synthesized at different active-site imprinting temperature.

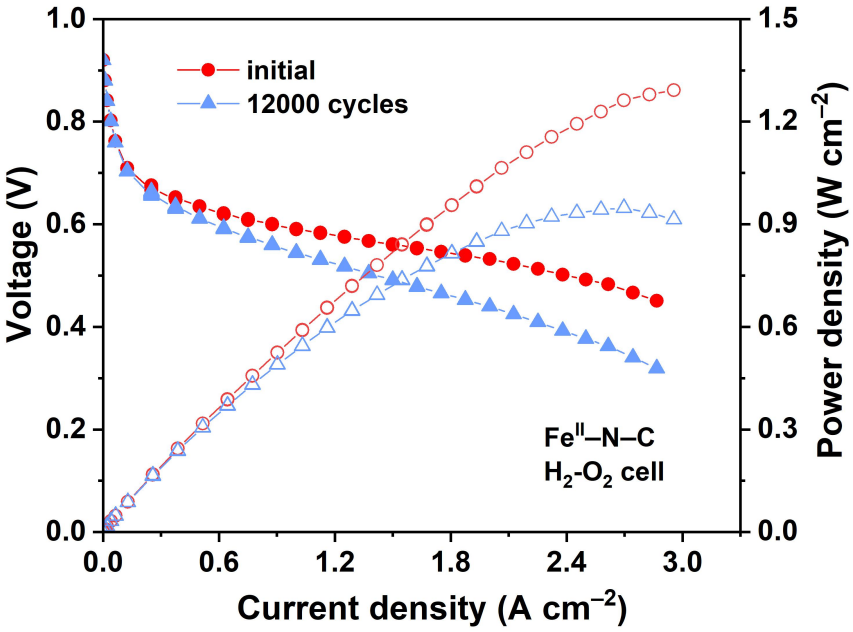

Figure S17. Polarization curves and power density curves of the optimal Fe^{II}–N–C catalyst before and after 12000 cycles under H_2–O_2 condition. Test conditions: The anode loading is 0.1 mg cm^{-2}, cathode loading is 4.0 mg cm^{-2}, relative humidity is 100 %, and the battery temperature is 80 °C.

Table S1. DFT calculated free energy for various slab models for Fe^{II}–N–C and Fe^{III}–N–C dual metal. The unit is eV.

	Slab 1 (ini)	Slab 2 (trans)	Slab 3 (fin)
$FeCl_2$-pyr-Zn	0	0.1408	–0.4191
$FeCl_2$-pyr-Vo	0	0.93	0.3505
$FeCl_3$-pyr-Zn	0	1.2285	0.1377
$FeCl_3$-pyr-Vo	0	1.8239	0.4695
$FeCl_2$-pyd-Zn	0		1.07742
$FeCl_2$-pyd-Vo	0		0.93305

Table S2. Curve fit Parameters for Fe^{II}–N–C and Zn–N–C K-edge EXAFS.

Sample	Path [a]	*N* [b]	*R* [c]/Å	σ^2 [d]/ Å^2	R factor/%
Zn foil [e]	Zn–Zn_1	6	2.64±0.01	0.012±0.001	0.9
	Zn–Zn_2	6	4.27±0.07	0.012±0.001	
Zn SAC [f]	Zn–N	4.3±0.8	2.02±0.01	0.008±0.002	1.4
Fe foil [g]	Fe–Fe_1	8	2.46±0.01	0.005±0.002	0.8
	Fe–Fe_2	6	2.88±0.01	0.004±0.002	
Fe SAC [h]	Fe–N	6.4±1.3	2.03±0.02	0.010±0.004	1.8

[a] The reference distances for Zn–Zn_1 (2.659 Å) and Zn–Zn_2 (3.940 Å) are from the crystal structure of Zn. The reference distances for Zn–N (1.972 Å) is from the crystal structure of ZnPc. The reference distances for Fe–Fe_1 (2.437 Å) and Fe–Fe_2 (2.814 Å) are from the crystal structure of Fe. The reference distances for Fe–N (1.925 Å) is from the crystal structure of FePc.

[b] *N* refers to the path degeneracy, which is identical to the coordination number for single-scattering paths. The *N* of Zn foil and Fe foil is fixed according to crystal structure of Zn and Fe, respectively.

[c] *R* refers to the distance to the scattering atoms.

[d] σ^2 refers to the Debye-Waller factor.

[e] S_0^2 was fitted as 0.97. ΔE_0 was refined as a global fit parameter, returning a value of (−1±1) eV. Data ranges: 3.0≤k≤12.0 Å^{-1}, 1.0≤R≤3.5 Å. The number of variable is 5, out of a total of 14.2 independent data points. The Debye-Waller factors were constrained as σ^2 (Zn–Zn$_1$) = σ^2 (Zn–Zn$_2$).

[f] S_0^2 was fixed as 0.97. ΔE_0 was refined as a global fit parameter, returning a value of (6±3) eV. Data ranges: 3.8≤k≤12.0 Å^{-1}, 1.2≤R≤2.5 Å. The number of variable is 4, out of a total of 6.5 independent data points.

[g] S_0^2 was fitted as 0.72. ΔE_0 was refined as a global fit parameter, returning a value of (5±2) eV. Data ranges: 2.0≤k≤12.0 Å^{-1}, 1.0≤R≤3.0 Å. The number of variable is 6, out of a total of 12.4 independent data points.

[h] S_0^2 was fixed as 0.72. ΔE_0 was refined as a global fit parameter, returning a value of (7±2) eV. Data ranges: 2.0≤k≤8.0 Å^{-1}, 1.0≤R≤2.8 Å. The number of variable is 4, out of a total of 6.7 independent data points.

Table S3. SD and $TOF_{0.3}$ values of Fe^{II}–N–C catalysts derived from the correlation of ORR kinetic activities measured in 0.5 M H_2SO_4 (j_{kin}, pH = 0.3) and site densities (measured by nitrite stripping at pH 0.3) in Fig.S8.

Catalyst	**SD (site g^{-1})**	**TOF (electrons site^{-1} s^{-1})**	
		@0.8V_{RHE}	@0.85V_{RHE}
Fe^{II}–N–C	4.27*1019	7.7	0.84
Fe–NC$^{\Delta-DCDA1}$	4.7*1019	5.4	0.84
Fe–N–C–CVD–750[2]	1.92*1020	0.8	/
Fe–N–C[3]	3.4*1019	1.63	/
FNCBSt–60[4]	3.26*1018	2.48	/
FNCBCO$_2$–5–950[4]	3.38*1018	3.9	/
P(1)*[5]	3.79*1019	1.49	/
Fe$_{0.5}$/NC fresh[6]	0.45*1019	7.1	/
ESG Fe–N–C[7]	6.98*1019	3.08	/

References

1 A. Mehmood, M. Gong, F. Jaouen, A. Roy, A. Zitolo, A. Khan, M.-T. Sougrati, M. Primbs, A. M. Bonastre, D. Fongalland, G. Drazic, P. Strasser and A. Kucernak, *Nature Catalysis*, 2022, **5**, 311-323.

2 L. Jiao, J. Li, L. L. Richard, Q. Sun, T. Stracensky, E. Liu, M. T. Sougrati, Z. Zhao, F. Yang, S. Zhong, H. Xu, S. Mukerjee, Y. Huang, D. A. Cullen, J. H. Park, M. Ferrandon, D. J. Myers, F. Jaouen and Q. Jia, *Nature Materials*, 2021, **20**, 1385-1391.

3 X. Wan, X. Liu, Y. Li, R. Yu, L. Zheng, W. Yan, H. Wang, M. Xu and J. Shui, *Nature Catalysis*, 2019, **2**, 259-268.

4 M. Mazzucato, G. Daniel, A. Mehmood, T. Kosmala, G. Granozzi, A. Kucernak and C. Durante, *Applied Catalysis B: Environmental*, 2021, **291**, 120068.

5 M. Liu, T. Sun, T. Peng, J. Wu, J. Li, S. Chen, L. Zhang, S. Li, J. Zhang and S. Sun, *ACS Energy Letters*, 2023, **8**, 4531-4539.

6 K. Kumar, L. Dubau, M. Mermoux, J. Li, A. Zitolo, J. Nelayah, F. Jaouen and F. Maillard, *Angewandte Chemie*, 2020, **132**, 3261-3269.

7 M. Liu, L. Wang, L. Zhang, Y. Zhao, K. Chen, Y. Li, X. Yang, L. Zhao, S. Sun and J. Zhang, *Small*, 2022, **18**, 2104934.